AlScN thin film based surface acoustic wave devices with enhanced microfluidic performance

W. B. Wang[a,b,c], Y. Q. Fu,[b,*] J. J. Chen,[c] W. P. Xuan[a], J. K. Chen[a], X. Z. Wang[a], P. Mayrhofer[d], P. F. Duan,[c] A. Bittner[d], U. Schmid[d] and J. K. Luo[e, a*]

a. Dept. of Info. Sci. & Electr. Eng., Zhejiang University and Cyrus Tang Century for Sensor Materials and Applications, 38 Zheda Road, Hangzhou 310027, China
b. Faculty of Eng. & Environ., University of Northumbria, Newcastle upon Tyne, NE1 8ST, UK
c. School of Mech. & Sys. Eng., Newcastle University, Newcastle Upon Tyne, NE1 7RU, UK
d. Inst. of Sensor & Actuator Systems, Vienna University of Technology, Floragasse 7, 1040 Vienna, Austria
e. Inst. of Renew. Energ. & Environ. Technol., University of Bolton, Deane Road, Bolton, BL3 5AB, UK

Abstract: This paper reports characterization of scandium aluminum nitride ($Al_{1-x}Sc_xN$, x = 27%)) films and its based surface acoustic wave (SAW) devices. Both AlScN and AlN films were deposited on silicon by sputtering and possessed columnar microstructures with (0002) crystal orientation. The AlScN/Si SAW devices showed an improved electromechanical coefficients (K^2, ~2%) compared with those of pure AlN films (<0.5%). The performance of the two types of devices, with acoustofluidic as an example, is also investigated and compared. Much lower threshold powers for both acoustic streaming and pumping of liquid droplets are achieved for the AlScN/Si SAW devices, acoustic streaming velocity is doubled and the pumping velocity is tripled compared with those using the AlN/Si SAW devices. Mechanical characterization shows that Young's modulus and hardness of the AlN film decrease significantly when Sc is doped, and is responsible for the decreased acoustic velocity, resonant frequency and increased temperature coefficient of frequency of the AlScN SAW devices.

Key word: AlScN**,** surface acoustic wave, microfluidics.

*Corresponding author emails: Richard.fu@northumbria.ac.uk; J.Luo@bolton.ac.uk.

1. Instruction

It is well reported that surface acoustic wave (SAW) devices can be utilized to fabricate sensors, actuator, and microfluidics and lab-on-chip systems with functions of sensing, actuating, streaming,

pumping, jetting, particle manipulation and nebulization *etc* [1-9]. Most of these SAW devices were made on bulk piezoelectric materials such as $LiNbO_3$ due to their good performance [5, 7]. However, the relatively brittle nature and high cost of substrate materials, as well as difficulty in integration with CMOS process could limit their applications. Thin film acoustic wave devices based on piezoelectric thin film materials, such as zinc oxide (ZnO) and aluminum nitride (AlN), are considered to be the future technology for the acoustic wave based sensors, microfluidics and lab-on-chips [3, 6, 10, 11]. Using thin films, rather than expensive bulk materials, it is convenient to integrate microelectronics and multiple sensing and microfluidics techniques into a lab-on-chip with low cost and multiple functions on various substrates (*e.g.* silicon, glass, metal, or polymer) [7, 12-15].

Currently, piezoelectric thin films such as ZnO have been extensively explored for SAW based sensors and microfluidics [6, 7, 16]. AlN, another extensively used piezoelectric film materials in micro-electro mechanical system (MEMS), has great advantages such as high acoustic velocity, outstanding stability at high temperatures, excellent chemical inertness and good compatibility with CMOS process [17]. It is one of the most important piezoelectric materials for many applications including energy harvesting [18], MEMS [19], sensors [20, 21] and acoustic wave devices, *etc* [10, 22, 23]. Currently AlN based SAW devices and film bulk acoustic resonator (FBAR) devices have been widely explored for sensors and actuators applications [24]. However, its relatively low electromechanical coupling coefficient (K^2) compared with those of the other materials (*e.g.*, $LiNbO_3$, PZT, ZnO *etc*.) limits its successful applications in sensor, actuator and microfluidics [22, 25-27].

Recently, it was reported that AlScN alloy with a high concentration of scandium (Sc) can significantly improve its piezoelectric properties [28-30]. Akiyama *et al*. reported that AlScN with 43% Sc showed an increase of piezoelectric moduli (d_{33}) by over 400% [28]. Based on *ab initio* simulation, Tasnádi *et al*. revealed that the increase of crystal cell volume causes the elastic softening and rise of d_{33} values [29, 30]. Using 46% Sc-alloyed AlN, Hashimoto *et al*. fabricated Sezewa mode SAW devices on AlScN/SiC substrate and demonstrated that its value of electromechanical coefficients can be increased up to 4% [31]. In our previous work, K^2 value for the Rayleigh SAW mode can be enhanced more than 300% when incorporating a 27% Sc element in AlScN [32, 33]. The significant improvement of K^2 value can be expected to lead to a higher efficiency for sensing, actuation and microfluidic applications, which will provide a promising opportunity for making better integrated lab-on-chips.

Current research on this topic has been focused on the understanding of physical mechanisms of scandium doping and enhancement of piezoelectric property, with few in-depth explorations for applications in sensors, actuators and microfluidics. In this study, we characterize the film properties and K^2 value and explore application of the AlScN thin film based SAW devices, with main focus on

microfluidics, and compare with those from the AlN based SAW microfluidics, proved that the AlScN based devices can provide much superior performance in microfluidics applications.

Doping of Sc in AlN would affect the mechanical strength of the films, consequently the integrity, reliability and stability of micro-devices for long-term application. However it is not clear whether the change of the mechanical strength by Sc-doping would affect and is correlated to the properties of the AlScN SAW devices. Since elastic softening is the main cause responsible for the enhancement of piezoelectric property, investigation on the Sc doping induced hardness change is therefore, important and useful for understanding physical mechanisms and applications of devices. Here we also report the characterization of the mechanical properties of the films by nanoindentation, and their effects on SAW devices of the Sc-alloyed AlN films. This may also provide valuable guidelines for optimizing the design of coatings on the devices and structures [34].

2. Experimental details

Thin films of AlScN and AlN were deposited on Si (100) substrate with a thickness of ~3 μm using DC reactive sputtering. AlScN thin films were deposited with a ScAl alloy target at a plasma power of 400 W and a base pressure in the deposition chamber of ~0.25 Pa without external substrate heating. AlN films were deposited using an Al target with nitrogen gas pressure of ~0.2 Pa, and the plasma power was set to be 800 W. Detailed deposition conditions were reported in our previous work [33, 35, 36]. Post annealing of the films were performed at 800 °C with a duration of 10 min, under nitrogen protection with a N_2 gas flow rate of 1 L/min.

Scanning electron microscope (SEM, Hitachi SU70, Japan) and atomic force microscope (AFM, SPI-3800N, Seiko Co., Japan) were used to characterize thin film microstructures and morphologies. X-ray photoelectron spectroscopy (XPS, K-Alpha, Thermo Scientific, UK) was performed using a monochromatic Al Kα X-ray source (1486.6 eV, 36 W) with an X-ray voltage of 12 kV.

Nanoindentation tests were performed using a Hysitron Triboindenter (Hysitron Inc. Nanomechanical Test Instruments, Minneapolis, MN, USA) with a Berkovich indenter. Displacement control protocol was adopted to investigate the depth-dependent properties. In this protocol, the loading and unloading rates were all 15 nm/s, and the penetration depth was increased from 15 nm to 100 nm. For each test, at least 10 indentations were performed and the average readings of elastic modulus and hardness were obtained using the Oliver and Pharr method [37].

SAW devices were fabricated on these thin film samples and the Ti/Au (5 and 60 nm thickness, respectively) interdigital transducers (IDT) were fabricated using a standard photolithograph and lift-off process. The wavelength of the devices was set to be 20 μm, with a delay line of 20 λ.

Characterization of frequencies of the SAW devices was conducted using a network analyzer (Agilent E5071C) [33].

For microfluidic tests, a signal generator (Marconi 2024) and a power amplifier (Amplifier research, 75A250) were utilized to generate and amplify the RF signals before applied to the SAW device, which was put on a bulk Al holder for easy heat dissipation. For microfluidic experiments, a hydrophobic layer of CYTOP (Asahi Glass Co. Ltd.) with ~200 nm thickness was deposited on the SAW devices. Water droplets of 2 μL were used, which was put about 2 mm in front of IDTs. Both acoustic streaming and droplet motion were captured by a high speed camera (Grasshopper 03K2C, 200 fps) and analyzed by software to obtain the velocities. The temperature coefficients of frequency (TCF) were measured in the temperature range of 30 °C to 90 °C for both the AlN and AlScN SAW devices. The temperature of the SAW devices was controlled on a probe station (Vector MX1100) which is capable of varying temperature up to 150 °C with a precision down to 0.1 °C. The temperature was further checked with an IR camera.

3. Results and discussions

XPS survey scans of both the AlN and AlScN thin films are shown in Fig. 1(a). Carbon peak appears at ~284.6 eV, which is due to the carbon contamination from the air and residual gaseous carbon-species in sputter chamber. The strong O 1s peaks of both the samples are linked to the residual oxygen in the gas atmosphere during sputtering and air contamination. The N 1s peak is positioned at ~396.8 eV.

Doping AlN with scandium results in a series of Sc 2p peaks at around 400-410 eV. The Sc 2p peak shown in Fig. 1(b) consists of two distinct sub-peaks. According to literature [38], the first peak from ~400.3 eV to 403.0 eV is related to Sc 2p3/2. The peak at ~400.3 eV is associated with metallic scandium. The large peak positioned at ~402.2 eV is a composite peak with the combination of both Sc 2p3/2 of Sc-N and Sc-O bond [38, 39], implying that part of Sc elements substituting Al atoms form covalent bonds with N and O. Similarly, the broad peak centered at ~406.5 eV is a composite peak of Sc 2p1/2 binding energy, with two main components, one of them is metallic Sc 2p1/2, and another one is a combined one from both Sc 2p1/2 of Sc-N and Sc-O bond [38]. The N 1s peak shown in Fig. 1(c) demonstrates a ~1.0 eV blue-shift of binding energy after doping with scandium which is due to the combination of Sc-N and Al-N bonds [39]. Figs. 1(d) and 1(e) illustrate slight blue-shift of the binding energy for the O 1s and Al 2p peaks, possibly caused by disturbance of the Sc doping. The oxygen peak is mainly related to the molecules adsorbed on the surface and they are less affected by scandium doping. On the other hand, incorporation of Sc has led to a minor shift of Al to the lower energy side, which indicates that the involvement of the Sc atoms slightly changes the ratio of Al-O and Al-N binding.

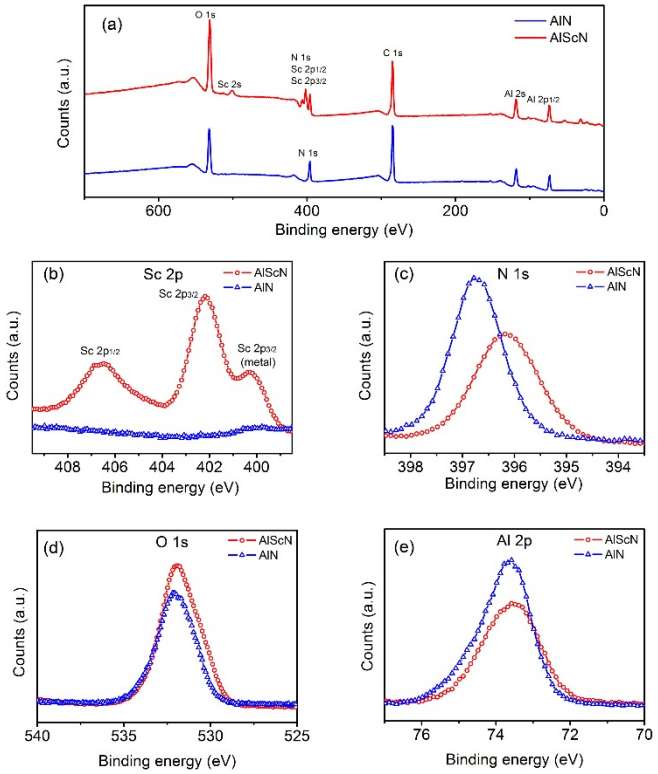

Figure 1. Comparison of XPS survey scans of AlN and AlScN thin films with binding energy range of 0-800 eV (a). The main peaks are identified and the presence of Sc is evident from the Sc 2p peaks with a binding energy of ~400 eV. And the detailed scanning of main peaks of AlScN and AlN: Sc 2p peaks around 400 eV (a), N 1s (b), O 1s (c) and Al 2p (d).

SEM micrographs in Figs. 3(a) and 3(b) show the fine microstructures of both the films and a columnar microstructure can be clearly observed from the cross-sectional view in Fig. 3(c). The surface morphology of AlScN films is slightly rougher and more irregular compared with that of pure AlN samples. Nevertheless, the results indicate that a heavy scandium doping will result in uniform growth and Sc elements will distribute uniformly in the crystal structures. XRD results reported in our previous work showed a good (0002) texture for both the films [33]. Smooth surface and columnar microstructure with a (0002) texture are beneficial for piezoelectric properties and acoustic wave device applications, and can reduce scattering effects and wave propagation loss.

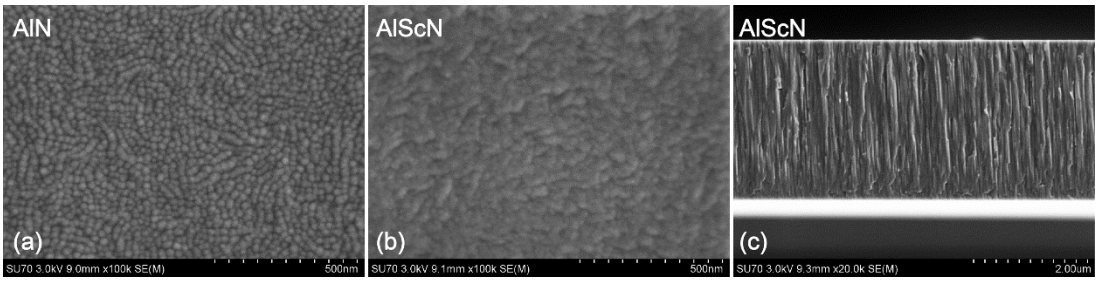

Figure 2. SEM image: top view of AlN (a), AlScN (b) thin film and cross sectional view of AlScN (c) sample.

Hardness and Young's modulus values for these two different types of samples are plotted in Fig. 3, as a function of indentation depth. As commented in ref. 40, the nanoindentation results would be significantly affected by the surface roughness when the indentation depth is below five times of the surface roughness [40]. Therefore, the indentation results for very small penetration (less than 20 nm) were discarded. There are several methods that enable determining the Young's modulus and hardness of thin coatings based on nanoindentation tests [8, 9, 27, 41-43]. Among these, the extrapolation of measured elastic modulus and hardness values of the coated systems to zero contact depth based on ISO14577 standard is simple and effective [41], and has been adopted for study here. As shown in Fig. 3, the values of Young's modulus and hardness of AlN film are ~209 GPa and 16.4 GPa respectively, which are higher than what were reported in ref. 42. This may suggest that the AlN films produced in this work have denser structure compared to the films reported [42]. AlN is one of the hardest materials with the Young's modulus of ~345 GPa [44, 45]. The value of ~210 GPa obtained in this work is much smaller than the one for bulk AlN material probably due to the unoptimized deposition condition, and thin film and polycrystalline nature, but much larger than 110.4 GPa reported in ref. 42 for which the deposition process and films may not be optimized at all.

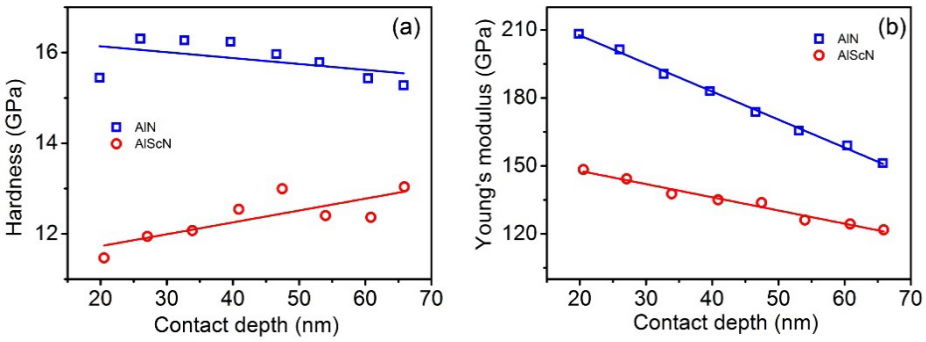

Figure 3. Comparison of the mechanical property: hardness (a) and Young's modulus (b). The data was obtained from nanoindentation tests.

The Young's modulus and hardness of the Sc doped AlN film are 149.4 GPa and 11.5 GPa, respectively, much lower than those of AlN films. Many theoretical researches indicate there is a softening effect of the Sc doping [29, 41], but may depend on the Sc concentration. Yang *et al* reported that at low Sc doping concentrations, Sc may form the Sc-N phase and restrict the growth of AlN grains [42]. The new Sc-N phase can act as a barrier to dislocation propagation which would enhance the hardness. However, further doping may lead to grain size decreased, and the grain boundary shearing begins to dominate the dislocation motion and the hardness will then decrease [46, 47]. The change trend of hardness with measurement depth for both the thin films is different, and is believed to be correlated to the hardness of Si substrate which is about 13 GPa, higher than that of

AlScN, but lower than that of AlN. With the increase in measurement depth, the effect of substrate becomes stronger, leading to opposite changes of the hardness with measurement depth.

Comparison of transmission spectra (S_{21}) of AlN and AlScN SAW devices is displayed in Fig. 4. It can be seen that after doping with scandium, the insertion loss of the AlScN film is significantly increased from ~-40 dB to ~-30 dB, and the peak amplitude is increased from ~17 dB to ~20 dB, implying that more acoustic energy has been transmitted, which could be beneficial for sensing, actuation and microfluidic applications. The resonant frequency also decreases slightly from 240 MHz for AlN SAW to 236.6 MHz for the Sc doped AlScN films. This corresponds to a decrease of the phase velocity from ~4800 m/s for AlN SAW to ~4730 m/s for the AlScN SAW. This is mainly due to the elastic softening after doping with Sc and change of crystal structure, consistent with the reduction of the mechanical strength obtained by nanoindentation shown above. The K^2 values were calculated using the following equation:

$$K^2 = \frac{\pi G_m(f_r)}{4NB_s(f_r)}$$

where N is the finger pairs, $G_m(f_r)$ and $B_s(f_r)$ are the motional conductance and static susceptance at the resonant frequency, fr, respectively, both the values were obtained from the Smith chart. K^2 values are shown in the inset of Fig. 4. For 20 μm devices discussed in this paper, with 27% Sc doping, the K^2 value increases from ~0.4% to ~2%, achieving more than 400% enhancement compared with those of the AlN SAW devices. The K^2 value of our AlScN films is also comparable to that of ZnO thin films (1~2%) [48], though slightly smaller than that of $LiNbO_3$ bulk materials (2~4%) [49]. The increase of K^2 value depends on the normalized thickness of the active layer, but all are more than 300% larger than that of AlN SAW as detailed in our previous work [33]. The great increase of the coupling coefficient is believed to be mainly caused by the significantly improved piezoelectric coefficient from elastic softening. This will significantly improve device performance, beneficial to sensor, actuator and microfluidic applications [33].

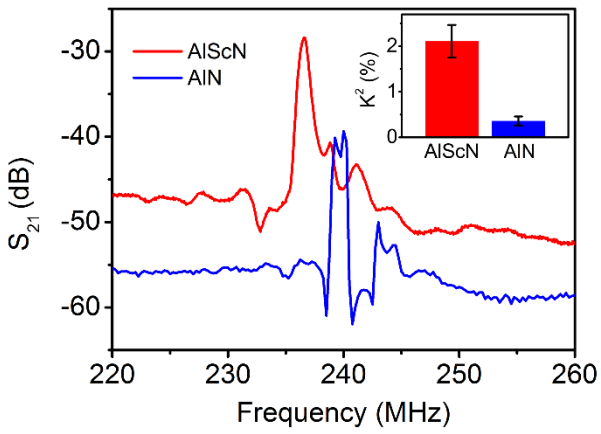

Figure 4. Comparison of transmission spectra (S_{21}) and K^2 values for AlN and AlScN devices with a wavelength of 20 μm.

To test this, we studied the acoustic wave based microfluidic phenomenon as an example for both the AlN and AlScN based SAW. Acoustic streaming can be easily obtained for both types of devices as shown in Fig. 5(a). The streaming was only confined in the localized wave/liquid interaction area in the droplet, especially for large droplets. This is because for such a high frequency SAW, the attenuation length is much shorter, and energy is dissipated easily in the front part of liquid droplet [2, 16]. Figs. 5(b) and 5(c) compare the threshold powers of streaming and the streaming velocities for the AlN and AlScN devices, respectively. The threshold power, defined as the minimum power that initiates the acoustic streaming, is a critical parameter for microfluidic applications. A lower threshold power means it is easier for the device to actuate liquid, having a higher efficiency and lower power dissipation. Fig. 5(b) demonstrates that with Sc doping, the threshold power of AlScN devices for streaming is ~40% that of AlN ones. This makes the AlScN SAW devices to produce much higher acoustic streaming velocity than that of AlN at the same powers. For instance, a 9 cm/s streaming velocity was obtained from AlScN SAW at an RF power of ~1.85 W, more than double of those (~4 cm/s) delivered by AlN SAW devices at the similar RF power [11, 16]. On the other hand, despite the much higher working frequency (~240 MHz), the AlN devices show a comparable threshold power value for streaming with those reported in literature (80.3 MHz AlN SAW) [22].

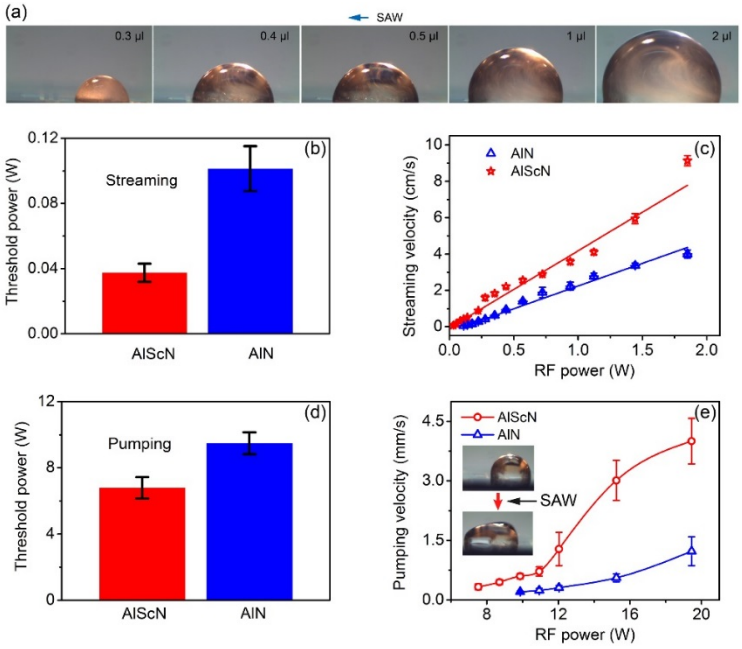

Figure 5 Photos of steaming phenomenon of AlScN based SAW devices with different droplet volumes (a), comparison of their threshold powers (b)(d), streaming velocities (c) and pumping velocities between AlN and AlScN SAW devices. The droplet volume was 2 μL for the comparison work.

We also studied the threshold power and pumping velocity of liquid droplet transportation for the two types of devices with the results shown in Fig. 5(d) and 5(e) respectively. Similar to acoustic streaming, the AlScN SAW devices present a much lower threshold power needed for pumping the droplets, and also achieve a higher velocity of pumping than that of the pure AlN SAW devices. With an RF power of 19.45 W, the AlScN SAW devices can achieve a droplet velocity of around 4 mm/s, which is 3 times higher than that of the AlN devices. Clearly, the enhancement of SAW microfluidic performance has been achieved by using scandium doped AlN SAW devices.

Temperature coefficient is an important value to estimate temperature stability of SAW devices, and increase in device temperature could shift the wave frequency, which could influence the resonant frequency, hence the performance of sensors, actuators and microfluidic devices during operation. Fig. 6 shows the frequency shift as a function of temperature, and the TCF values were calculated to be ~-31.0 ppm/K and ~-32.9 ppm/K for AlN and AlScN SAW device, respectively, that are consistent with those reported for the AlN SAW devices [25]. Significant doping with Sc in the AlN film only increases the TCF value slightly, but the trend is consistent with the reduced Young's modulus and hardness values for the AlScN films as shown above. The TCFs of both types of films are much smaller than those of ZnO and $LiNbO_3$ [13, 50]. It should be emphasized that low TCF would be important for acoustic wave resonators to maintain the stability or reliability during operation at high temperatures. A low TCF value with an excellent linearity will enable the AlScN based SAW devices to be employed for various sensing, actuation and microfluidic applications with better control and reliable results.

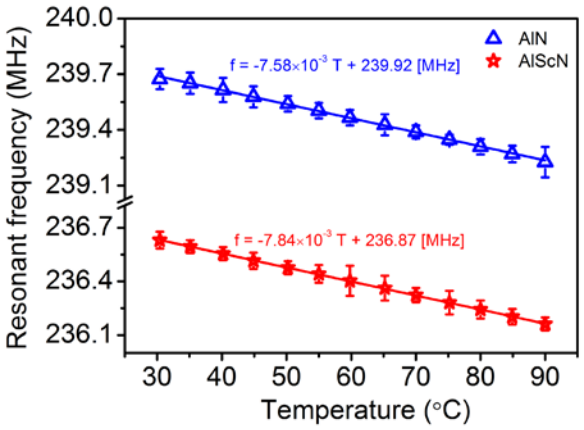

Figure 6 Resonant frequency as a function of temperature for both AlN and AlScN devices, the temperature region is 30-90℃.

4. Conclusions

In summary, both the AlN and AlScN thin films showed a smooth surface morphology and a columnar microstructure perpendicular to the substrate surface and good (0002) textures. AlScN

based SAW devices demonstrated higher electromechanical coefficients (~2%) compared with those based on AlN films (<1%). With high doping of scandium, significant softening effects (i.e. drop in Young's modulus and hardness) have been observed compared to those of pure AlN film, which is correlated to the increase in the TCF and decrease in the phase velocity (resonant frequency). As a consequence, the AlScN SAW devices showed a lower threshold power as well as a higher velocity for both streaming and droplet pumping, two major microfluidic functions, and demonstrated that scandium doping improved the acoustofluidic performance significantly. In addition, the nanoindentation results also suggest that deposition conditions may need further optimization to improve the microstructure of the coatings and thus the performance of the devices.

Acknowledgments:

Funding support from NSFC (61274037) and Royal Academy of Engineering: Research Exchange between UK and China was acknowledged. Wenbo Wang acknowledges the Lin Guangzhao & Hu Guozan Graduate Education International Exchange Fund for sponsoring his study at Newcastle University. X-ray photoelectron spectra were obtained at the National EPSRC XPS Users' Service (NEXUS) at Newcastle University, an EPSRC Mid-Range Facility. For Austria, we gratefully acknowledge the financial support from the Austrian Science Fund (FWF), number P 25212-N30 and EU COST program (IC-1208). In addition, Pengfei Duan acknowledges the PhD scholarship offered by Newcastle University. J. Chen is acknowledging funding from the Engineering and Physical Sciences Research Council (EP/K039083/1).

References

[1] Yeo L Y and Friend J R 2014 Surface Acoustic Wave Microfluidics *Annu. Rev. Fluid Mech.* **46** 379-406

[2] Schmid L, Wixforth A, Weitz D A and Franke T 2011 Novel surface acoustic wave (SAW)-driven closed PDMS flow chamber *Microfluid. Nanofluid.* **12** 229-35

[3] Yeo L Y and Friend J R 2009 Ultrafast microfluidics using surface acoustic waves *Biomicrofluidics* **3** 12002

[4] Shi J, Ahmed D, Mao X, Lin S C, Lawit A and Huang T J 2009 Acoustic tweezers: patterning cells and microparticles using standing surface acoustic waves (SSAW) *Lab Chip* **9** 2890-5

[5] Brodie D S, Fu Y Q, Li Y, Alghane M, Reuben R L and Walton A J 2011 Shear horizontal surface acoustic wave induced microfluidic flow *Appl. Phys. Lett.* **99** 153704

[6] Fu Y Q, Luo J K, Du X Y, Flewitt A J, Li Y, Markx G H, Walton A J and Milne W I 2010 Recent developments on ZnO films for acoustic wave based bio-sensing and microfluidic applications: a review *Sens. Actuators B* **143** 606-19

[7] Du X Y, Fu Y Q, Luo J K, Flewitt A J and Milne W I 2009 Microfluidic pumps employing surface acoustic waves generated in ZnO thin films *J. Appl. Phys.* **105** 024508

[8] Collins D J, Morahan B, Garcia-Bustos J, Doerig C, Plebanski M and Neild A 2015 Two-dimensional single-cell patterning with one cell per well driven by surface acoustic waves *Nat. Commun.* **6** 11

[9] Guo F, Mao Z M, Chen Y C, Xie Z W, Lata J P, Li P, Ren L Q, Liu J Y, Yang J, Dao M, Suresh S and Huang T J 2016 Three-dimensional manipulation of single cells using surface acoustic waves *Proc. Natl. Acad. Sci. USA* **113** 1522-7
[10] Wingqvist G 2010 AlN-based sputter-deposited shear mode thin film bulk acoustic resonator (FBAR) for biosensor applications — A review *Surf. Coat. Tech.* **205** 1279-86
[11] Du X Y, Fu Y Q, Tan S C, Luo J K, Flewitt A J, Milne W I, Lee D S, Park N M, Park J, Choi Y J, Kim S H and Maeng S 2008 ZnO film thickness effect on surface acoustic wave modes and acoustic streaming *Appl. Phys. Lett.* **93** 094105
[12] Liu Y, Li Y, el-Hady A M, Zhao C, Du J F, Liu Y and Fu Y Q 2015 Flexible and bendable acoustofluidics based on ZnO film coated aluminium foil *Sens. Actuators B* **221** 230-5
[13] Wang W, He X, Zhou J, Gu H, Xuan W, Chen J, Wang X and Luo J K 2014 Comparative Study on Microfluidic Performance of ZnO Surface Acoustic Wave Devices on Various Substrates *J. Electrochem. Soc.* **161** B230-B6
[14] Jin H, Zhou J, He X, Wang W, Guo H, Dong S, Wang D, Xu Y, Geng J, Luo J K and Milne W I 2013 Flexible surface acoustic wave resonators built on disposable plastic film for electronics and lab-on-a-chip applications *Sci. Rep.* **3** 2140
[15] Chen J, He X, Wang W, Xuan W, Zhou J, Wang X, Dong S R, Garner S, Cimo P and Luo J K 2014 Bendable transparent ZnO thin film surface acoustic wave strain sensors on ultra-thin flexible glass substrates *J. Mater. Chem. C* **2** 9109-14
[16] Guo Y J, Lv H B, Li Y F, He X L, Zhou J, Luo J K, Zu X T, Walton A J and Fu Y Q 2014 High frequency microfluidic performance of LiNbO3 and ZnO surface acoustic wave devices *J. Appl. Phys.* **116** 024501
[17] Caliendo C and Imperatori P 2003 High-frequency, high-sensitivity acoustic sensor implemented on ALN/Si substrate *Appl. Phys. Lett.* **83** 1641
[18] Elfrink R, Kamel T M, Goedbloed M, Matova S, Hohlfeld D, van Andel Y and van Schaijk R 2009 Vibration energy harvesting with aluminum nitride-based piezoelectric devices *J. Micromech. Microengin.* **19** 094005
[19] Taniyasu Y and Kasu M 2010 Surface 210 nm light emission from an AlN p–n junction light-emitting diode enhanced by A-plane growth orientation *Appl. Phys. Lett.* **96** 221110
[20] Wingqvist G, Bjurström J, Liljeholm L, Yantchev V and Katardjiev I 2007 Shear mode AlN thin film electro-acoustic resonant sensor operation in viscous media *Sens. Actuators B* **123** 466-73
[21] Kucera M, Wistrela E, Pfusterschmied G, Ruiz-Díez V, Manzaneque T, Hernando-García J, Sánchez-Rojas J, Jachimowicz A, Schalko J, Bittner A and Schmid U 2014 Design-dependent performance of self-actuated and self-sensing piezoelectric-AlN cantilevers in liquid media oscillating in the fundamental in-plane bending mode *Sens. Actuators B* **200** 235-44
[22] Zhou J, Pang H F, Garcia-Gancedo L, Iborra E, Clement M, De Miguel-Ramos M, Jin H, Luo J K, Smith S, Dong S R, Wang D M and Fu Y Q 2015 Discrete microfluidics based on aluminum nitride surface acoustic wave devices *Microfluid. Nanofluid.* **18** 537-48
[23] Zhou C J, Shu Y, Yang Y, Jin H, Dong S R, Chan M S and Ren T L 2015 Flexible structured high-frequency film bulk acoustic resonator for flexible wireless electronics *J. Micromech. Microengin.* **25** 055003
[24] Flewitt A J, Luo J K, Fu Y Q, Garcia-Gancedo L, Du X Y, Lu J R, Zhao X B, Iborra E, Ramos M and Milne W I 2015 ZnO based SAW and FBAR devices for bio-sensing applications *J. Non-Newton. Fluid* **222** 209-16
[25] Zhou J, DeMiguel-Ramos M, Garcia-Gancedo L, Iborra E, Olivares J, Jin H, Luo J K, Elhady A S, Dong S R, Wang D M and Fu Y Q 2014 Characterisation of aluminium nitride films and surface acoustic wave devices for microfluidic applications *Sens. Actuators B* **202** 984-92
[26] Zhou C J, Yang Y, Jin H, Feng B, Dong S R, Luo J K, Ren T L, Chan M S and Yang C Y 2013 Surface acoustic wave resonators based on (002)AlN/Pt/diamond/silicon layered structure *Thin Solid Films* **548** 425-8
[27] Zhou J, He X, Jin H, Wang W, Feng B, Dong S, Wang D, Zou G and Luo J K 2013 Crystalline structure effect on the performance of flexible ZnO/polyimide surface acoustic wave devices *J. Appl. Phys.* **114** 044502
[28] Akiyama M, Kamohara T, Kano K, Teshigahara A, Takeuchi Y and Kawahara N 2009 Enhancement of piezoelectric response in scandium aluminum nitride alloy thin films prepared by dual reactive cosputtering *Adv. Mater.* **21** 593-6
[29] Tasnádi F, Alling B, Höglund C, Wingqvist G, Birch J, Hultman L and Abrikosov I A 2010 Origin of the Anomalous Piezoelectric Response in Wurtzite $Sc_xAl_{1-x}N$ Alloys *Phys. Rev. Lett.* **104**
[30] Tholander C, Abrikosov I, Hultman L and Tasnádi F 2013 Volume matching condition to establish the enhanced piezoelectricity in ternary $(Sc,Y)_{0.5}(Al,Ga,In)_{0.5}N$ alloys *Phys. Rev. B* **87**

[31] Hashimoto K Y, Sato S, Teshigahara A, Nakamura T and Kano K 2013 High-performance surface acoustic wave resonators in the 1 to 3 GHz range using a ScAlN/6H-SiC structure *IEEE Trans. Ultrason. Ferroelectr. Freq. Control* **60** 637-42

[32] Mayrhofer P M, Euchner H, Bittner A and Schmid U 2015 Circular test structure for the determination of piezoelectric constants of Sc Al N thin films applying Laser Doppler Vibrometry and FEM simulations *Sens. Actuators A* **222** 301-8

[33] Wang W B, Mayrhofer P M, He X L, Gillinger M, Ye Z, Wang X Z, Bittner A, Schmid U and Luo J K 2014 High performance AlScN thin film based surface acoustic wave devices with large electromechanical coupling coefficient *Appl. Phys. Lett.* **105** 133502

[34] Chen J, Bull S J, Roy S, Mukaibo H, Nara H, Momma T, Osaka T and Shacham-Diamand Y 2008 Mechanical analysis and in situ structural and morphological evaluation of Ni–Sn alloy anodes for Li ion batteries *J. Phys. D* **41** 025302

[35] Mayrhofer P M, Eisenmenger-Sittner C, Stöger-Pollach M, Euchner H, Bittner A and Schmid U 2014 The impact of argon admixture on the c-axis oriented growth of direct current magnetron sputtered $Sc_xAl_{1-x}N$ thin films *J. Appl. Phys.* **115** 193505

[36] Schneider M, Bittner A, Patocka F, Stöger-Pollach M, Halwax E and Schmid U 2012 Impact of the surface-near silicon substrate properties on the microstructure of sputter-deposited AlN thin films *Appl. Phys. Lett.* **101** 221602

[37] Oliver W C and Pharr G M 1992 An improved technique for determining hardness and elastic modulus using load and displacement sensing indentation experiments *J. Mater. Res.* **7** 1564-83

[38] Biesinger M, Lau L, Gerson A and Smart R 2010 Resolving surface chemical states in XPS analysis of first row transition metals, oxides and hydroxides: Sc, Ti, V, Cu and Zn *Appl. Surf. Sci.* **257** 887-98

[39] NIST X-ray Photoelectron Spectroscopy Database, Version 4.1 (National Institute of Standards and Technology, Gaithersburg, 2012); http://srdata.nist.gov/xps/, 2012

[40] Chen J, Birch M A and Bull S J 2010 Nanomechanical characterization of tissue engineered bone grown on titanium alloy in vitro *J. Mater. Sci. Mater. Med.* **21** 277-82

[41] Moram M A and Zhang S 2014 ScGaN and ScAlN: emerging nitride materials *J. Mater. Chem. A* **2** 6042

[42] Yang J, Li Y, Cao M and Chen Y 2013 Structure and nanomechanical properties of $Al_{1-x}Sc_xN$ thin films *J. Phys.: Conf. Ser.* **419** 012035

[43] ISO 14577, Metallic materials—Instrumented indentation test for hardness and materials parameters—Part 4. Test method for metallic and non-metallic coatings, 2007, International Standards Organisation

[44] Andrei A, Krupa K, Jozwik M, Delobelle P, Hirsinger L, Gorecki C, Nieradko L and Meunier C 2008 AlN as an actuation material for MEMS applications *Sens. Actuators A* **141** 565-76

[45] Wright A F 1997 Elastic properties of zinc-blende and wurtzite AlN, GaN, and InN *J. Appl. Phys.* **82** 2833

[46] Carlton C E and Ferreira P J 2007 What is behind the inverse Hall–Petch effect in nanocrystalline materials? *Acta Materialia* **55** 3749-56

[47] Schiøtz J, Tolla F D D and Jacobsen K W 1998 Softening of nanocrystalline metals at very small grain sizes *Nature* **391** 561-3

[48] Zhou J, He X L, Wang W B, Zhu Q, Xuan W P, Jin H, Dong S R, Wang D M and Luo J K 2013 Transparent Surface Acoustic Wave Devices on ZnO/Glass Using Al-Doped ZnO as the Electrode *IEEE Electr Device L.* **34** 1319-21

[49] Cheng C C, Horng R C and Chen Y C 2001 Formation and properties of proton-exchanged and annealed LiNbO3 waveguides for surface acoustic wave *IEEE Trans. Ultrason. Ferroelectr. Freq. Control* **48** 387-91

[50] Du X Y, Swanwick M E, Fu Y Q, Luo J K, Flewitt A J, Lee D S, Maeng S and Milne W I 2009 Surface acoustic wave induced streaming and pumping in 128° Y-cut LiNbO3for microfluidic applications *J. Micromechan. Microengin.* **19** 035016